Inorg. Chem. **2004**, *43*, 6734–6744

Density Functional Investigation of Metal–Metal Interactions in Mixed-Valence d^2d^3 (Cr, Mo, W) and d^3d^4 (Mn, Tc, Re) Face-Shared $[M_2Cl_9]^{2-}$ Systems

Germán Cavigliasso, Peter Comba,† and Robert Stranger*

Department of Chemistry, Faculty of Science, Australian National University, Canberra ACT 0200, Australia

Received April 16, 2004

The molecular and electronic structures of mixed-valence face-shared (Cr, Mo, W) d^2d^3 and (Mn, Tc, Re) d^3d^4 $[M_2Cl_9]^{2-}$ dimers have been calculated by density functional methods in order to investigate metal–metal bonding in this series. The electronic structures of these systems have been analyzed using potential energy curves for the broken-symmetry and other spin states arising from the d^2d^3 and d^3d^4 coupling modes. In (d^2d^3) $[Mo_2Cl_9]^{2-}$ and $[W_2Cl_9]^{2-}$, the global minimum has been found to be a spin-doublet state characterized by delocalization of the metal-based electrons in a multiple metal–metal bond (with a formal bond order of 2.5). In contrast, weak coupling between the metal centers and electron localization are favored in (d^2d^3) $[Cr_2Cl_9]^{2-}$, the global minimum for this species being a ferromagnetic $S = 5/2$ state with a relatively long Cr–Cr separation. The (d^3d^4) $[Re_2Cl_9]^{2-}$ system also exhibits a global minimum corresponding to a metal–metal bonded spin-doublet state with a formal bond order of 2.5, reflecting the electron–hole equivalence between d^2d^3 and d^3d^4 configurations. Double minima behavior is predicted for (d^3d^4) $[Tc_2Cl_9]^{2-}$ and $[Mn_2Cl_9]^{2-}$ due to two energetically close low-lying states (these being $S = 3/2$ and $S = 5/2$ states for the former, and $S = 5/2$ and $S = 7/2$ states for the latter). A comparison of computational results for the d^2d^2, d^2d^3, and d^3d^3 $[W_2Cl_9]^{z-}$ series and the d^3d^3, d^3d^4, and d^4d^4 $[Re_2Cl_9]^{z-}$ series indicates that the observed trends in metal–metal distances can only be rationalized if changes in both the strength of σ bonding and metal–metal bond order are taken into consideration. These two factors act conjointly in the W series but in opposition to one another in the Re series. In the case of the $[Cr_2Cl_9]^{z-}$ and $[Mn_2Cl_9]^{z-}$ dimers, the metal–metal bond lengths are significantly shorter for mixed-valence (d^2d^3 or d^3d^4) than d^3d^3 systems. This result is consistent with the fact that some degree of metal–metal bonding exists in the former (due to partial delocalization of a single σ electron) but not in the latter (where all metal-based electrons are completely localized).

1. Introduction

In a series of recent publications[1−8] we have explored metal−metal interactions in a wide variety of face-shared dinuclear $[M_2X_9]^{z-}$ systems, which include 3d, 4d, and 5d transition metals with d^1d^1, d^2d^2, d^3d^3, d^4d^4, and d^5d^5 electronic configurations.

This extensive series of $[M_2X_9]^{z-}$ dimers is characterized by a diverse range of metal−metal interactions. In species of the second (4d) and third (5d) transition series, the interactions between metal d orbitals are the dominant factor, and these systems typically exhibit strong covalent metal−metal bonds. However, in general, metals of the first (3d) transition series have large spin polarization (or exchange) energies, and this has a more significant effect on the electronic structure than the (orbital) interaction between adjacent metal centers, leading to localized electron distributions and weakly coupled metal atoms in species such as $[V_2Cl_9]^{3-}$ and $[Cr_2Cl_9]^{3-}$.

* Author to whom correspondence should be addressed. E-mail: rob.stranger@anu.edu.au.

† Permanent address: Institute of Inorganic Chemistry, University of Heidelberg, D-69120 Heidelberg, Germany.

(1) Lovell, T.; McGrady, J. E.; Stranger, R.; Macgregor, S. A. *Inorg. Chem.* **1996**, *35*, 3079.
(2) McGrady, J. E.; Stranger, R.; Lovell, T. *J. Phys. Chem. A* **1997**, *101*, 6265.
(3) Stranger, R.; McGrady, J. E.; Lovell, T. *Inorg. Chem.* **1998**, *37*, 6795.
(4) Lovell, T.; Stranger, R.; McGrady, J. E. *Inorg. Chem.* **2001**, *40*, 39.
(5) Stranger, R.; Turner, A.; Delfs, C. D. *Inorg. Chem.* **2001**, *40*, 4093.
(6) Petrie, S.; Stranger, R. *Polyhedron* **2002**, *21*, 1163.
(7) Stranger, R.; Lovell, T.; McGrady, J. E. *Polyhedron* **2002**, *21*, 1969.
(8) Cavigliasso, G.; Stranger, R. *Inorg. Chem.* **2004**, *43*, 2368.

10.1021/ic049503m CCC: $27.50
Published on Web 09/18/2004

In systems with d^1d^1, d^2d^2, and d^3d^3 configurations,[1−3,5] the electrons involved in metal−metal interactions can be associated with the t_{2g} orbitals of a regular octahedral $[MX_6]^{z-}$ complex. For species possessing a d^4d^4 or d^5d^5 configuration,[4,7,8] the metal−metal interaction also depends on whether a "high-spin" or "low-spin" configuration is adopted. These two cases are related, respectively, to the metal-based electrons occupying solely the t_{2g} orbitals or being distributed over both the t_{2g} and e_g orbitals in an octahedral monomer. The heavier members of the d^4d^4 and d^5d^5 series (which contain 4d and 5d metals) are characterized by low-spin configurations and strong coupling between the metal centers, as a result of metal−metal bond formation. In contrast, the corresponding 3d systems feature weakly coupled high-spin metal centers with $S = 4$ or $S = 5$ ground states, corresponding to localization of the metal-based electrons.

The wide range of bonding possibilities makes the theoretical and computational treatment of the electronic structures of these $[M_2X_9]^{z-}$ dimers especially challenging. Nevertheless, we have shown in our previous publications[1−8] that density functional theory in combination with the broken-symmetry approach[9,10] can accurately describe the entire range of metal−metal interactions, from weak antiferromagnetic coupling through to strong multiply bonded metal centers, as well as encompassing both high-spin and low-spin metal configurations.

The success of this procedure can be exemplified by noting that our broken-symmetry density functional calculations have accurately reproduced experimentally observed properties not only for the most typical examples of face-shared $[M_2X_9]^{z-}$ dimers, represented by the d^3d^3 systems formed by Cr, Mo, and W, but also for species displaying more "complicated" electronic structures such as the d^2d^2 $[V_2Cl_9]^{3-}$ and $[Nb_2Cl_9]^{3-}$ and d^5d^5 $[Ru_2Cl_9]^{3-}$ dimers.

In this article, we extend our computational investigations of face-shared $[M_2X_9]^{z-}$ dimers by calculating the molecular and electronic structures of species possessing mixed-valence d^2d^3 and d^3d^4 configurations. The present study is focused on systems which have been crystallographically characterized,[11,12] namely $[W_2Cl_9]^{2-}$ and $[Re_2Cl_9]^{2-}$, but the analogous Cr, Mo, Mn, and Tc species, and the $[W_2Br_9]^{2-}$ system (whose crystal structure has been reported[13]), are also considered. Although not structurally characterized, the preparation, spectral, and magnetic properties of $[Mo_2Cl_9]^{2-}$ have been discussed in the literature.[14−16]

The description and analysis of the electronic structures of these dimers are carried out by exploring the potential energy curves for the broken symmetry and other spin states corresponding to several possible coupling modes of the metal centers. Calculations on the $[Re_2Cl_9]^{2-}$ system have been previously carried out using the Xα method,[12] but detailed computational studies of the structure and bonding in mixed-valence face-shared $[M_2X_9]^{z-}$ dimers, involving potential energy curves and full geometry optimizations, have not been reported.

2. Calculation Details

All density-functional calculations reported in this article were carried out with the ADF (2002.03) program.[17−19] Functionals based on the Volko-Wilk-Nusair[20] (VWN) form of the Local Density Approximation[21] (LDA) were utilized, and no gradient corrections or relativistic effects were included as previous work has shown that these normally result in poorer agreement with experimental structural data.[2] Basis sets of triple-ζ quality and one polarization function (TZP or type IV), incorporating frozen cores (Cl.2p, Br.3p, and M.2p, M.3d, M.4f for the first, second, and third transition series, respectively), were employed.[17−19]

Calculations on the $[M_2Cl_9]^{2-}$ systems were carried out using the (full) D_{3h} molecular symmetry, with the exception of the broken-symmetry calculations which employed C_{3v} symmetry. It should be noted that the main goal of this work is the qualitative description and understanding of trends in metal−metal interactions in d^2d^3 and d^3d^4 species, and, therefore, calculations were performed only on the broken-symmetry and spin states which were considered to be most relevant to the analysis of the electronic structures of these systems (but not on all possible states arising from the various d^2d^3 and d^3d^4 coupling modes).

Some test calculations using the COSMO solvation model[22] were carried out on W and Re systems, and no significant changes in the structural parameters or in the qualitative energy trends were observed. Incorporating this solvation treatment considerably increases the computational demands and costs (relative to an "isolated molecule" approach), and therefore this methodology was not used in the calculation of potential energy curves or in related geometry optimizations.

3. Results and Discussion

In a number of recent publications,[2−8] we have shown that a satisfactory description of the entire range of metal−metal interactions in face-shared $[M_2X_9]^{z-}$ dimers can be achieved by means of an approach based on analyzing the broken-symmetry potential energy curves in terms of the curves for the associated spin states. These arise when one or more subsets of metal-based electrons are engaged in metal−metal bonding.

The molecular structure of face-shared $[M_2X_9]^{z-}$ dimers (Figure 1) exhibits ideal D_{3h} geometry. Imposing symmetry breaking on this structure results in the lowering of the molecular symmetry from D_{3h} to C_{3v} as a consequence of

(9) Noodleman, L.; Norman, J. G. *J. Chem. Phys.* **1979**, *70*, 4903.
(10) Noodleman, L. *J. Chem. Phys.* **1981**, *74*, 5737.
(11) Cotton, F. A.; Falvello, L. R.; Mott, G. N., Schrock, R. R.; Sturgeoff, L. G. *Inorg. Chem.* **1983**, *22*, 2621.
(12) Heath, G. A.; McGrady, J. E.; Raptis, R. G.; Willis, A. C. *Inorg. Chem.* **1996**, *35*, 6838.
(13) Templeton, J. L., Jacobson, R. A., McCarley, R. E. *Inorg. Chem.* **1977**, *16*, 3320.
(14) Delphin, W. H.; Wentworth, R. A. D. *J. Am. Chem. Soc.* **1973**, *95*, 7920.
(15) Delphin, W. H.; Wentworth, R. A. D.; Matson, M. S. *Inorg. Chem.* **1974**, *13*, 2552.
(16) Trogler, W. C. *Inorg. Chem.* **1980**, *19*, 697.
(17) ADF, SCM, Theoretical Chemistry, Vrije Universiteit, Amsterdam, The Netherlands (http://www.scm.com).
(18) Fonseca Guerra, C.; Snijders, J. G.; te Velde, G.; Baerends, E. J. *Theor. Chem. Acc.* **1998**, *99*, 391.
(19) te Velde, G.; Bickelhaupt, F. M.; Baerends, E. J.; Fonseca Guerra, C.; van Gisbergen, S. J. A.; Snijders, J. G.; Ziegler, T. *J. Comput. Chem.* **2001**, *22*, 931.
(20) Vosko, S. H.; Wilk, L.; Nusair, M. *Can. J. Phys.* **1980**, *58*, 1200.
(21) Kohn, W.; Sham, L. J. *Phys. Rev.* **1965**, *140*, A1133.
(22) Pye, C. C.; Ziegler, T. *Theor. Chem. Acc.* **1999**, *101*, 396.

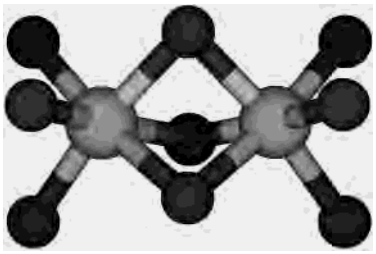

Figure 1. Molecular structure of face-shared $[M_2X_9]^{z-}$ systems.

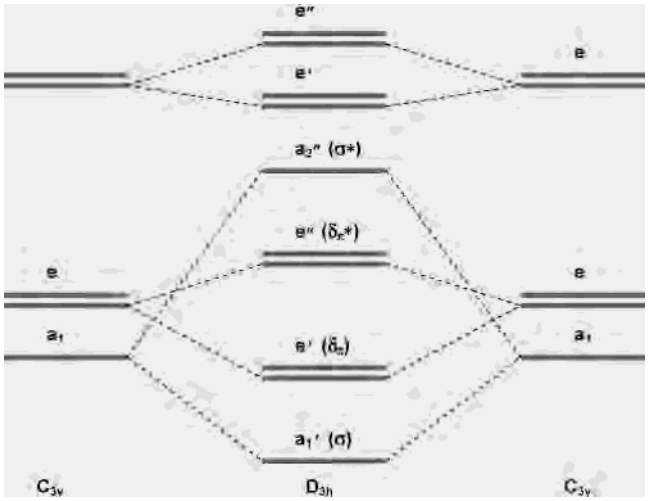

Figure 2. Schematic representation of the correlation between metal-based molecular orbitals in C_{3v} (broken-symmetry) and D_{3h} (full-symmetry) descriptions.

removing all symmetry elements connecting the metal centers. The correlation between C_{3v} and D_{3h} molecular orbital descriptions is shown in Figure 2.

The connection between the (C_{3v}) broken-symmetry and the (D_{3h}) associated states can be made by noting that when antiferromagnetic coupling within a subset of electrons is weak, then the corresponding ferromagnetic associated state, where the weakly coupled electrons are aligned in parallel, must lie close in energy. The most representative example is probably found for the d^3d^3 $[M_2X_9]^{z-}$ dimers.[2,5] In these systems, the associated states arise from successive decoupling of the σ and δ_π subsets of electrons and correspond to $S = 0$, $S = 2$, and $S = 3$ configurations, all of which can be represented by single-determinant wave functions. The $S = 0$, $S = 2$, and $S = 3$ states are characterized, respectively, by delocalization of all electrons, delocalization of the σ, but not δ_π, electrons, and localization of all electrons.

It should be noted that, except in the case of complete delocalization of all metal-based electrons, the broken-symmetry state does not correspond to the true ground state but to a weighted average of the pure spin states arising from the coupling between the two metal centers. Although this spin-contamination problem can be addressed using approximate spin-projection techniques, we have shown in a previous publication[2] that, when considering the general features of a potential energy curve, approximate spin projection is not necessary because the broken-symmetry curve closely follows that for the true ground state at all points.

The local C_{3v} symmetry of the metal sites in the $[M_2X_9]^{z-}$ dimers splits the t_{2g} set of orbitals in an ideal octahedral ($[MX_6]^{z-}$) complex into a_1 and e subsets. For d^3d^3 species, the "natural" occupancy of these levels corresponds to the $[(a_1)^1(e)^2]$ single-ion configuration, giving rise to only one coupling mode. For d^2d^3 and d^3d^4 systems, however, several single-ion configurations are possible, resulting in a number of different coupling modes.

The potential energy curves for the broken-symmetry and associated states corresponding to various d^2d^3 and d^3d^4 coupling modes are described in Sections 3.1 through 3.3. The (crystallographically characterized) $[W_2Cl_9]^{2-}$ and $[Re_2Cl_9]^{2-}$ dimers are explored in detail, and results for the analogous Cr, Mo, Mn, and Tc systems, and for $[W_2Br_9]^{2-}$, are also discussed.

3.1. Potential Energy Curves for d^2d^3 $[M_2Cl_9]^{2-}$ Systems. Two coupling modes, denoted $[a_1e \times a_1e^2]$ and $[e^2 \times a_1e^2]$, are relevant to d^2d^3 $[M_2Cl_9]^{2-}$ dimers and correspond to the electrons associated with the d^2 metal center residing in both the a_1 and e orbitals or exclusively in the e orbitals, respectively. Schematic representations for the electronic configurations of the broken-symmetry and associated spin states (Table 1), for both coupling modes, are given in Figure 3, and plots of the potential energy curves are shown in Figures 4 and 5. Optimized metal−metal distances and total bonding energies corresponding to the minima in the potential energy curves are summarized in Table 2.

In the $[a_1e \times a_1e^2]$ coupling mode, the broken-symmetry state corresponds to the $[(a_1\uparrow)^1(a_1\downarrow)^1(e\uparrow)^1(e\downarrow)^2(e\uparrow)^0(e\downarrow)^0(a_1\uparrow)^0(a_1\downarrow)^0]$ (C_{3v}) configuration. The potential energy curve for this broken-symmetry state can be discussed in terms of $S = 1/2$, $S = 3/2$, and $S = 5/2$ spin states (Figure 4), which correspond to antiferromagnetic coupling of both σ and δ_π electrons, antiferromagnetic coupling of σ electrons but ferromagnetic coupling of δ_π electrons, and ferromagnetic coupling of both σ and δ_π electrons.

For the $[e^2 \times a_1e^2]$ coupling mode, the broken-symmetry state is defined by the $[(a_1\uparrow)^0(a_1\downarrow)^1(e\uparrow)^2(e\downarrow)^2(e\uparrow)^0(e\downarrow)^0(a_1\uparrow)^0(a_1\downarrow)^0]$ (C_{3v}) configuration. The potential energy curve for this broken-symmetry state can be analyzed by considering $S = 1/2$ and $S = 5/2$ spin states (Figure 4), which arise from antiferromagnetic and ferromagnetic alignment of the δ_π electrons, respectively.

3.1.1. Coupling Modes and Potential Energy Curves for $[W_2Cl_9]^{2-}$. The potential energy curves for the broken-symmetry and associated spin states belonging to the (d^2d^3) $[a_1e \times a_1e^2]$ and $[e^2 \times a_1e^2]$ coupling modes (described in the preceding section) are shown in Figure 4 for the $[W_2Cl_9]^{2-}$ system.

For the $[a_1e \times a_1e^2]$ coupling mode, the broken-symmetry curve lies close to the $S = 5/2$ state at long metal−metal distances, indicating electron localization, whereas at short metal−metal distances, it converges toward the $S = 1/2$ state where electron delocalization occurs as a result of the formation of σ (a_1') and δ_π (e′) bonds. In the intermediate range of metal−metal separations, the $S = 3/2$ state lies lower in energy than both the $S = 1/2$ and $S = 5/2$ states and closest to the broken-symmetry curve. Therefore, at intermediate

Table 1. Electronic Configurations and Multiplets Arising from the Coupling Modes of d^2d^3 and d^3d^4 $[M_2Cl_9]^{2-}$ Systems[a]

coupling mode		configuration	spin state	multiplets
d^2d^3	$[a_1e \times a_1e^2]$	$[(a_1'\uparrow)^1(a_1'\downarrow)^1(e'\uparrow)^1(e'\downarrow)^2(e''\uparrow)^0(e''\downarrow)^0(a_2''\uparrow)^0(a_2''\downarrow)^0]$	S = 1/2	$^2\mathbf{E}'$
		$[(a_1'\uparrow)^1(a_1'\downarrow)^1(e'\uparrow)^2(e'\downarrow)^0(e''\uparrow)^1(e''\downarrow)^0(a_2''\uparrow)^0(a_2''\downarrow)^0]$	S = 3/2	$^4\mathbf{E}''$
		$[(a_1'\uparrow)^1(a_1'\downarrow)^0(e'\uparrow)^2(e'\downarrow)^0(e''\uparrow)^1(e''\downarrow)^0(a_2''\uparrow)^1(a_2''\downarrow)^0]$	S = 5/2	$^6\mathbf{E}'$
	$[e^2 \times a_1e^2]$	$[(a_1'\uparrow)^1(a_1'\downarrow)^0(e'\uparrow)^2(e'\downarrow)^2(e''\uparrow)^0(e''\downarrow)^0(a_2''\uparrow)^0(a_2''\downarrow)^0]$	S = 1/2	$^2\mathbf{A_1}'$
		$[(a_1'\uparrow)^1(a_1'\downarrow)^0(e'\uparrow)^2(e'\downarrow)^0(e''\uparrow)^2(e''\downarrow)^0(a_2''\uparrow)^0(a_2''\downarrow)^0]$	S = 5/2	$^6\mathbf{A_1}'$
		$[(a_1'\uparrow)^1(a_1'\downarrow)^0(e'\uparrow)^2(e'\downarrow)^1(e''\uparrow)^1(e''\downarrow)^0(a_2''\uparrow)^0(a_2''\downarrow)^0]$	S = 3/2′	$^4A_1' + {}^4A_2' + {}^4E''$
		$[(a_1'\uparrow)^0(a_1'\downarrow)^1(e'\uparrow)^2(e'\downarrow)^0(e''\uparrow)^2(e''\downarrow)^0(a_2''\uparrow)^0(a_2''\downarrow)^0]$	S = 3/2″	$^4A_1'$
d^3d^4	$[a_1e^2 \times a_1{}^2e^2]$	$[(a_1'\uparrow)^1(a_1'\downarrow)^1(e'\uparrow)^2(e'\downarrow)^2(e''\uparrow)^0(e''\downarrow)^0(a_2''\uparrow)^1(a_2''\downarrow)^0]$	S = 1/2	$^2\mathbf{A_2}''$
		$[(a_1'\uparrow)^1(a_1'\downarrow)^1(e'\uparrow)^2(e'\downarrow)^2(e''\uparrow)^0(e''\downarrow)^0(a_2''\uparrow)^1(a_2''\downarrow)^0]$	S = 5/2	$^6\mathbf{A_2}''$
		$[(a_1'\uparrow)^1(a_1'\downarrow)^1(e'\uparrow)^2(e'\downarrow)^1(e''\uparrow)^1(e''\downarrow)^0(a_2''\uparrow)^1(a_2''\downarrow)^0]$	S = 3/2′	$^4A_1' + {}^4A_2' + {}^4E'$
		$[(a_1'\uparrow)^1(a_1'\downarrow)^1(e'\uparrow)^2(e'\downarrow)^0(e''\uparrow)^2(e''\downarrow)^0(a_2''\uparrow)^0(a_2''\downarrow)^1]$	S = 3/2″	$^4A_2''$
	$[a_1e^2 \times a_1e^3]$	$[(a_1'\uparrow)^1(a_1'\downarrow)^1(e'\uparrow)^2(e'\downarrow)^2(e''\uparrow)^1(e''\downarrow)^0(a_2''\uparrow)^0(a_2''\downarrow)^0]$	S = 1/2	$^2\mathbf{E}''$
		$[(a_1'\uparrow)^1(a_1'\downarrow)^1(e'\uparrow)^2(e'\downarrow)^1(e''\uparrow)^2(e''\downarrow)^0(a_2''\uparrow)^0(a_2''\downarrow)^0]$	S = 3/2	$^4\mathbf{E}'$
		$[(a_1'\uparrow)^1(a_1'\downarrow)^0(e'\uparrow)^2(e'\downarrow)^1(e''\uparrow)^2(e''\downarrow)^0(a_2''\uparrow)^1(a_2''\downarrow)^0]$	S = 5/2	$^6\mathbf{E}''$
		$[(a_1'\uparrow)^1(a_1'\downarrow)^0(e'\uparrow)^2(e'\downarrow)^0(e''\uparrow)^2(e''\downarrow)^0(a_2''\uparrow)^1(a_2''\downarrow)^0(e'\uparrow))^1(e'\downarrow)^0]$	S = 7/2	$^8\mathbf{E}''$

[a] The energy of the multiplets highlighted in bold type can be calculated using a single-determinant approach.

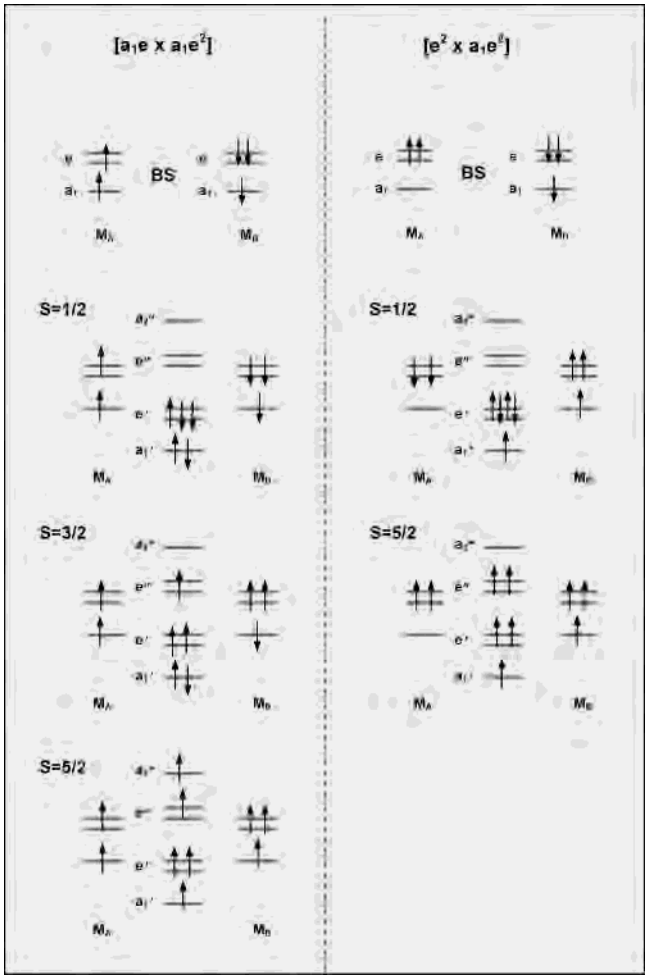

Figure 3. Schematic representation of the electronic configurations for the broken symmetry and spin states associated with the $[a_1e \times a_1e^2]$ and $[e^2 \times a_1e^2]$ coupling modes of d^2d^3 $[M_2Cl_9]^{2-}$ systems.

W−W distances, the metal−metal interactions can be described as involving a σ bond but weakly coupled δ_π electrons. The minimum in the broken-symmetry curve for the $[a_1e \times a_1e^2]$ coupling mode coincides with that of the S = 1/2 state, both occurring at a W−W separation of 2.56 Å and corresponding to multiple metal−metal bonding, with a formal bond order of 2.5 (represented by $[1.0\ \sigma + 1.5\ \delta_\pi]$).

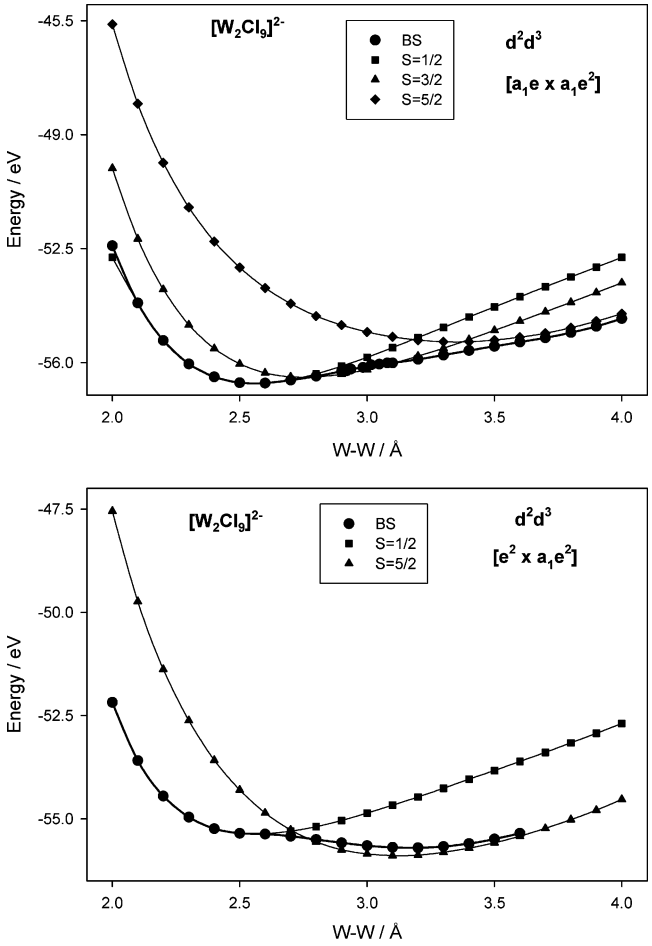

Figure 4. Potential energy curves for (d^2d^3) $[W_2Cl_9]^{2-}$.

For the $[e^2 \times a_1e^2]$ coupling mode, the broken-symmetry state lies close to the S = 5/2 state at intermediate to long metal−metal distances but converges toward the S = 1/2 state, characterized by a formal bond order of 2.5 (corresponding to $[0.5\ \sigma + 2.0\ \delta_\pi]$), at metal−metal separations shorter than 2.7 Å. The minimum in the S = 5/2 curve is close to that of the broken-symmetry curve and energetically lower than the minimum for the S = 1/2 state, indicating that localization of the metal-based electrons is favored in this coupling mode.

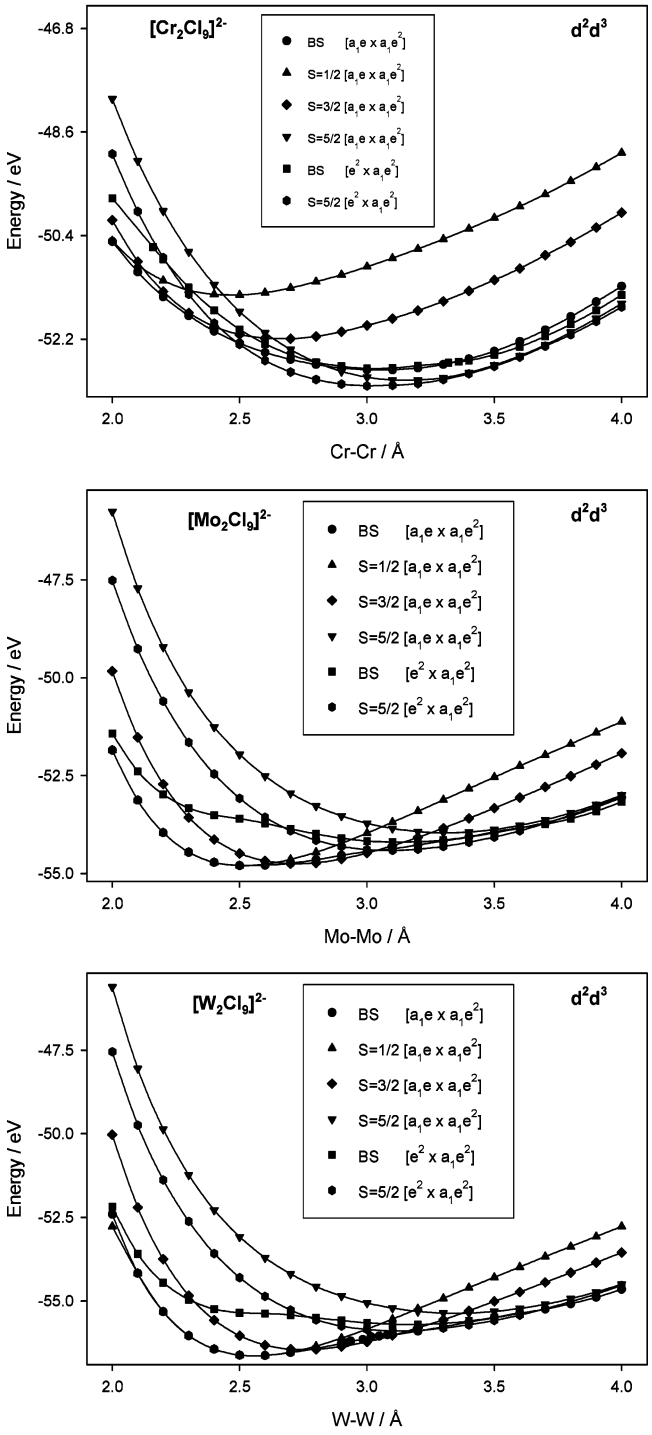

Figure 5. Potential energy curves for (d^2d^3) $[Cr_2Cl_9]^{2-}$, $[Mo_2Cl_9]^{2-}$, and $[W_2Cl_9]^{2-}$.

A comparison of the structural data for the S = 5/2 states, for both the $[a_1e \times a_1e^2]$ and $[e^2 \times a_1e^2]$ coupling modes (Table 2), reveals that the metal−metal distance in the latter is predicted to be approximately 0.24 Å shorter than in the former (a similar result being observed for $[Cr_2Cl_9]^{2-}$ and $[Mo_2Cl_9]^{2-}$). This difference can be rationalized on the basis that although both S = 5/2 states are characterized by a formal metal−metal bond order of 0.5, the metal−metal interaction involves δ_π bonding in the $[a_1e \times a_1e^2]$ coupling mode but σ bonding in the $[e^2 \times a_1e^2]$ coupling mode (Figure 3).

Table 2. Optimized Metal−Metal Bond Distance (M−M in Å) and Total Bonding Energy (E_B in eV) for the Broken Symmetry and Spin States Belonging to the $[a_1e \times a_1e^2]$ and $[e^2 \times a_1e^2]$ Coupling Modes of (d^2d^3) $[Cr_2Cl_9]^{2-}$, $[Mo_2Cl_9]^{2-}$, and $[W_2Cl_9]^{2-}$

molecule	coupling mode	state	M−M	E_B
$[Cr_2Cl_9]^{2-}$	$[a_1e \times a_1e^2]$	BS	3.085	−52.76
		S = 1/2	2.468	−51.43
		S = 3/2	2.648	−52.19
		S = 5/2	3.155	−52.92
	$[e^2 \times a_1e^2]$	BS	3.027	−52.73
		S = 1/2	2.687	−50.62
		S = 5/2	3.015	−53.01
		S = 3/2′	2.906	−51.34
		S = 3/2″	2.977	−52.14
$[Mo_2Cl_9]^{2-}$	$[a_1e \times a_1e^2]$	BS	2.511	−54.80
		S = 1/2	2.507	−54.80
		S = 3/2	2.717	−54.75
		S = 5/2	3.313	−53.96
	$[e^2 \times a_1e^2]$	BS	3.139	−54.21
		S = 1/2	2.523	−53.58
		S = 5/2	3.099	−54.41
		S = 3/2′	2.851	−53.50
		S = 3/2″	3.057	−53.94
$[W_2Cl_9]^{2-}$	$[a_1e \times a_1e^2]$	BS	2.562	−56.64
		S = 1/2	2.559	−56.64
		S = 3/2	2.756	−56.45
		S = 5/2	3.350	−55.36
	$[e^2 \times a_1e^2]$	BS	3.162	−55.71
		S = 1/2	2.562	−55.37
		S = 5/2	3.114	−55.89
		S = 3/2′	2.879	−55.13
		S = 3/2″	3.114	−55.48

In addition to the S = 1/2 and S = 5/2 associated states, two S = 3/2 states (denoted S = 3/2′ and S = 3/2″ in Tables 1 and 2) can be defined for the $[e^2 \times a_1e^2]$ coupling mode. However, both S = 3/2 curves lie energetically higher than the S = 5/2 state and are, thus, not relevant to the discussion of the global minimum of d^2d^3 $[M_2Cl_9]^{2-}$ species.

3.1.2. General Analysis of the Potential Energy Curves. The potential energy curves for the states which are most important in determining the global minima of $[Cr_2Cl_9]^{2-}$, $[Mo_2Cl_9]^{2-}$, and $[W_2Cl_9]^{2-}$, and for a comparative discussion of the most significant similarities and differences, are collected in Figure 5.

The potential energy curves for $[Mo_2Cl_9]^{2-}$ and $[W_2Cl_9]^{2-}$ are qualitatively similar, the behavior of both systems being characterized by a preference for metal−metal bond formation. However, significant differences are observed in the potential energy curves for $[Cr_2Cl_9]^{2-}$ since, in contrast to the Mo and W dimers, electron localization plays a more predominant role.

The global minimum for both $[Mo_2Cl_9]^{2-}$ and $[W_2Cl_9]^{2-}$ occurs at a short metal−metal separation and corresponds to the S = 1/2 state arising from the $[a_1e \times a_1e^2]$ coupling mode. The reported experimental W−W bond length is 2.54 Å[11] and is closely reproduced by the present calculations, the predicted value being 2.56 Å. The metal−metal interaction at the global minimum for the Mo and W dimers can be described as electron delocalization in a Mo−Mo or W−W multiple bond, with a formal bond order of 2.5 (corresponding to $[1.0\ \sigma + 1.5\ \delta_\pi]$). Despite the general (qualitative) similarities between the Mo and W systems, it is important to note that while in $[W_2Cl_9]^{2-}$ the S = 1/2 state appears to be more clearly favored over any other ($[a_1e$

$\times$ a_1e^2] or [e^2 $\times$ a_1e^2]) states, in $[Mo_2Cl_9]^{2-}$ the ([a_1e $\times$ a_1e^2]) S = 1/2 and S = 3/2 minima are (energetically) noticeably closer (with the gap predicted to be only 0.05 eV).

The computational results for $[Mo_2Cl_9]^{2-}$ are consistent with the observed magnetic properties. Experimental studies[14,15] of the temperature dependence of the magnetic moments indicate that the ground state of this species should correspond to the S = 1/2 state but that the S = 3/2 state is also thermally populated at room temperature.

The potential energy curve for the S = 1/2 state arising from the [a_1e $\times$ a_1e^2] coupling mode is the lowest-lying curve at metal−metal distances shorter than approximately 2.6 Å ($[Mo_2Cl_9]^{2-}$) or 2.8 Å ($[W_2Cl_9]^{2-}$), but it shifts to higher energy as the metal−metal separation increases. In the intermediate range of metal−metal distances investigated (which corresponds to 2.7−3.1 Å for $[Mo_2Cl_9]^{2-}$ and 2.8−3.2 Å for $[W_2Cl_9]^{2-}$), the S = 3/2 state belonging to the [a_1e $\times$ a_1e^2] coupling mode lies lowest in energy, but at longer metal−metal separations the S = 5/2 states (belonging to both the [a_1e $\times$ a_1e^2] and [e^2 $\times$ a_1e^2] coupling modes) become energetically favored.

Unlike the Mo and W systems, the global minimum in $[Cr_2Cl_9]^{2-}$ occurs at a relatively long metal−metal separation of 3.02 Å, and corresponds to the S = 5/2 state arising from the [e^2 $\times$ a_1e^2] coupling mode. This minimum can be characterized as involving a predominantly localized electron distribution and weakly coupled metal centers. The potential energy curve for this state lies lowest in energy at all Cr−Cr distances greater than 2.5 Å, and the two S = 5/2 curves (from the [a_1e $\times$ a_1e^2] and [e^2 $\times$ a_1e^2] coupling modes) are actually almost coincident at Cr−Cr separations longer than approximately 3.3 Å. The ([a_1e $\times$ a_1e^2]) S = 3/2 and S = 1/2 states are energetically favored only at the shortest metal−metal distances investigated.

3.2. General Results for d^2d^3 $[W_2Br_9]^{2-}$. The synthesis and structural characterization of the d^2d^3 $[W_2Br_9]^{2-}$ dimer was reported many years ago.[13] The W−W distance is 2.601 Å, and a small (angular) distortion from the ideal D_{3h} symmetry was found and attributed to Jahn−Teller effects.

Analogously to the $[M_2Cl_9]^{2-}$ systems, we have calculated potential energy curves for the [a_1e $\times$ a_1e^2] and [e^2 $\times$ a_1e^2] broken-symmetry and associated states of $[W_2Br_9]^{2-}$. The computational results predict that the ground state for this dimer should correspond to the S = 1/2 state arising from the [a_1e $\times$ a_1e^2] coupling mode (as also found for $[W_2Cl_9]^{2-}$) and that the W−W distance should be 2.603 Å, in excellent agreement with the experimental observation.

In addition to the general calculations on D_{3h} structures, we have explored the possibility of observing Jahn−Teller distortions by lowering the molecular symmetry to C_{2v}. This causes the orbital degeneracy associated with the $(e')^3$ electron occupancy in the ([a_1e $\times$ a_1e^2]) S = 1/2 state to be removed, by splitting the e′(D_{3h}) level into a_1 and b_2 (C_{2v}) orbitals. Although earlier researchers[13] have acknowledged that the e′ orbitals of the (D_{3h}) $[M_2Cl_9]^{2-}$ systems can be considered "modified t_{2g}" orbitals and that no significant Jahn−Teller effects should therefore be expected, these authors have suggested that this is the most likely reason for the observed distortions in $[W_2Br_9]^{2-}$.

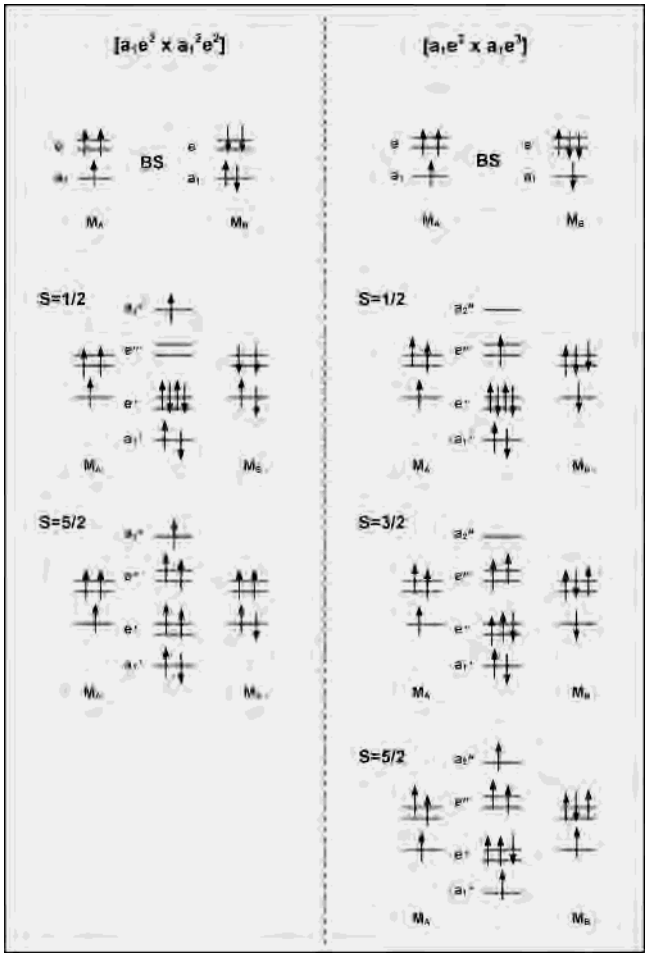

Figure 6. Schematic representation of the electronic configurations for the broken symmetry and spin states associated with the [a_1e^2 $\times$ $a_1^2e^2$] and [a_1e^2 $\times$ a_1e^3] coupling modes of d^3d^4 $[M_2Cl_9]^{2-}$ systems.

Our calculations on $[W_2Br_9]^{2-}$, employing C_{2v} symmetry, indicate that there are only slight changes in the structural parameters (approximately 0.01 Å for bond distances and 1−3 degrees for bond angles), and no significant stabilization has been found, the energetic difference between the D_{3h} and C_{2v} forms predicted to be less than 0.01 eV. In addition, further reduction of the molecular symmetry to C_s has led to only minor changes relative to the D_{3h} or C_{2v} results.

The calculated W−Br bond lengths and Br−W−Br bond angles are in good agreement with the reported (average) experimental values, with the deviations between computational and crystallographic results being approximately 0.02−0.03 Å for distances and 1.0 degree for angles.

3.3. Potential Energy Curves for d^3d^4 $[M_2Cl_9]^{2-}$ Systems. The description of the coupling modes and broken-symmetry and associated states for d^3d^4 $[M_2Cl_9]^{2-}$ dimers is analogous to that presented for d^2d^3 systems due to the fact that the d^4 configuration can be considered the "hole" equivalent of the d^2 configuration. The two coupling modes for d^3d^4 dimers are denoted [a_1e^2 $\times$ $a_1^2e^2$] and [a_1e^2 $\times$ a_1e^3] and correspond, respectively, to the electron holes associated with the d^4 metal center residing exclusively in the e orbitals or in both a_1 and e orbitals.

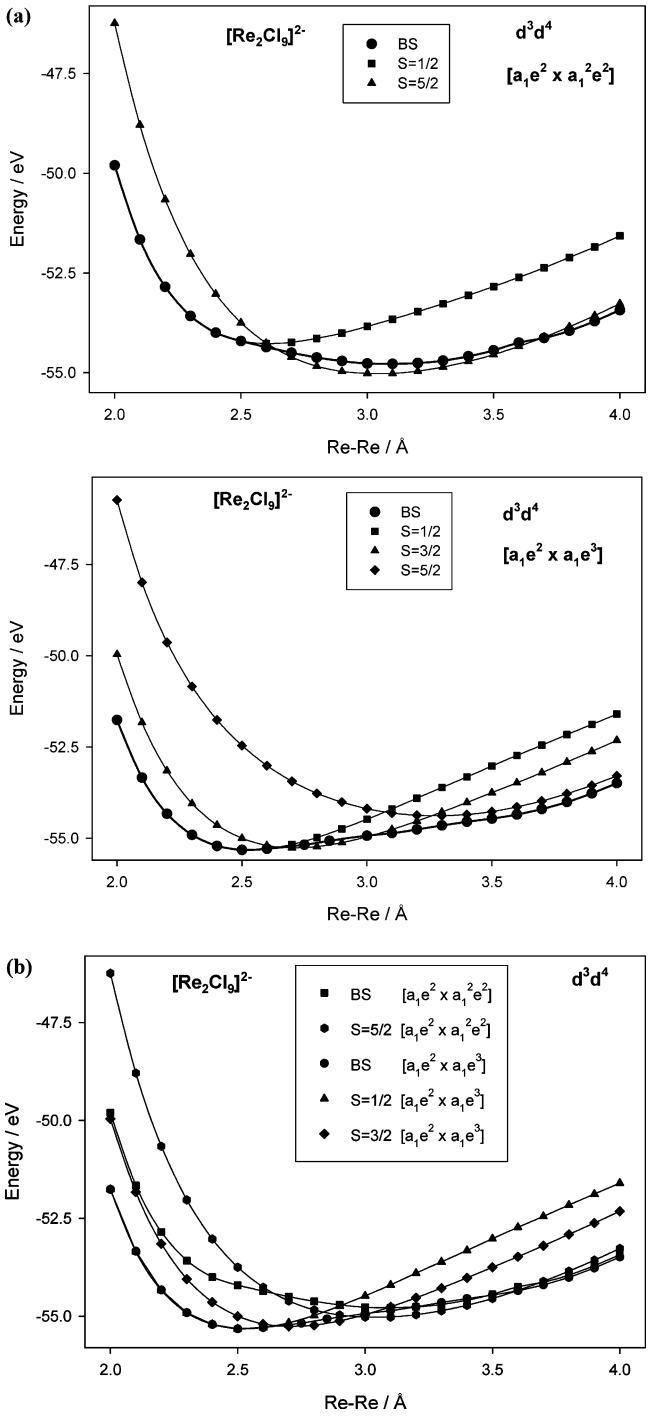

Figure 7. Potential energy curves for (d^3d^4) $[Re_2Cl_9]^{2-}$.

Schematic representations for the electronic configurations of the broken-symmetry and associated spin states (Table 1) for both coupling modes are given in Figure 6, and plots of the potential energy curves are shown in Figures 7 and 8. Optimized metal−metal distances and total bonding energies corresponding to the minima in the potential energy curves are summarized in Table 3.

3.3.1. Coupling Modes and Potential Energy Curves for $[Re_2Cl_9]^{2-}$. The potential energy curves for the $[a_1e^2 \times a_1{}^2e^2]$ and $[a_1e^2 \times a_1e^3]$ broken-symmetry and associated spin states of $[Re_2Cl_9]^{2-}$ are shown in section (a) of Figure 7.

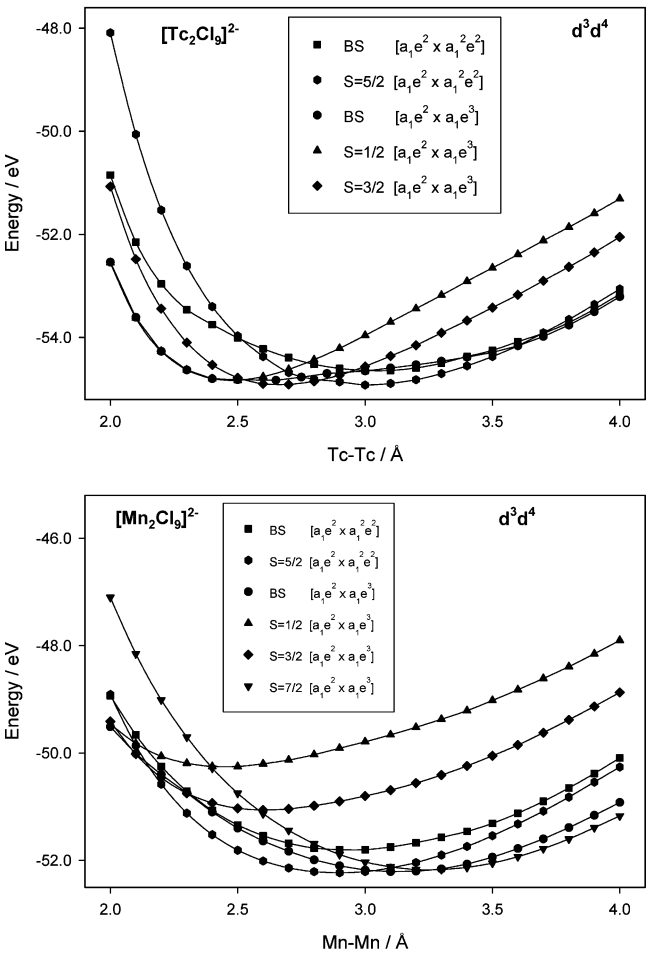

Figure 8. Potential energy curves for (d^3d^4) $[Tc_2Cl_9]^{2-}$ and $[Mn_2Cl_9]^{2-}$.

Table 3. Optimized Metal−Metal Bond Distance (M−M in Å) and Total Bonding Energy (E_B in eV) for the Broken Symmetry and Spin States Belonging to the $[a_1e^2 \times a_1{}^2e^2]$ and $[a_1e^2 \times a_1e^3]$ Coupling Modes of (d^3d^4) $[Mn_2Cl_9]^{2-}$, $[Tc_2Cl_9]^{2-}$, and $[Re_2Cl_9]^{2-}$

molecule	coupling mode		state	M−M	E_B
$[Mn_2Cl_9]^{2-}$	$[a_1e^2 \times a_1{}^2e^2]$		BS	2.941	−51.81
			S = 1/2	2.681	−49.83
			S = 5/2	2.891	−52.23
			S = 3/2′	2.813	−50.62
			S = 3/2″	2.917	−51.16
	$[a_1e^2 \times a_1e^3]$		BS	3.165	−52.29
		low spin	S = 1/2	2.417	−50.25
			S = 3/2	2.594	−51.06
			S = 5/2	3.070	−51.91
		high spin	S = 7/2	3.238	−52.17
$[Tc_2Cl_9]^{2-}$	$[a_1e^2 \times a_1{}^2e^2]$		BS	3.041	−54.65
			S = 1/2	2.566	−53.88
			S = 5/2	2.994	−54.92
			S = 3/2′	2.813	−54.02
			S = 3/2″	2.996	−54.33
	$[a_1e^2 \times a_1e^3]$		BS	2.539	−54.85
			S = 1/2	2.485	−54.83
			S = 3/2	2.661	−54.92
			S = 5/2	3.210	−54.34
$[Re_2Cl_9]^{2-}$	$[a_1e^2 \times a_1{}^2e^2]$		BS	3.100	−54.78
			S = 1/2	2.604	−54.27
			S = 5/2	3.038	−55.03
			S = 3/2′	2.848	−54.27
			S = 3/2″	3.037	−54.51
	$[a_1e^2 \times a_1e^3]$		BS	2.514	−55.32
			S = 1/2	2.522	−55.32
			S = 3/2	2.710	−55.26
			S = 5/2	3.255	−54.38

The broken-symmetry state for the $[a_1e^2 \times a_1{}^2e^2]$ coupling mode is defined by the $[(a_1\uparrow)^1(a_1\downarrow)^1(e\uparrow)^2(e\downarrow)^2(e\uparrow)^0(e\downarrow)^0(a_1\uparrow)^1(a_1\downarrow)^0]$ (C_{3v}) configuration (Figure 6). The potential energy

curve for this broken-symmetry state can be analyzed by considering S = 1/2 and S = 5/2 spin states (Figure 7), arising, respectively, from antiferromagnetic and ferromagnetic alignment of the δ_π electrons.

The $[a_1e^2 \times a_1^2e^2]$ broken-symmetry state lies close to the S = 5/2 state at intermediate to long metal−metal distances but converges with the S = 1/2 state at metal−metal separations shorter than 2.6 Å. The minimum in the S = 5/2 curve (at 3.04 Å) is close to that of the broken-symmetry curve and energetically lower than the minimum for the S = 1/2 state, indicating a preference for localization of the metal-based electrons in this coupling mode. Analogous to the d^2d^3 $[M_2Cl_9]^{2-}$ systems, S = 3/2′ and S = 3/2″ states can also be defined for the $[a_1e^2 \times a_1^2e^2]$ coupling mode of the d^3d^4 dimers. However, the S = 3/2 curves lie energetically higher than the S = 5/2 state (Table 3) and are not an option for the ground state of $[Re_2Cl_9]^{2-}$.

For the $[a_1e^2 \times a_1e^3]$ coupling mode, the broken-symmetry state corresponds to the $[(a_1\uparrow)^1(a_1\downarrow)^1(e\uparrow)^2(e\downarrow)^2(e\uparrow)^1(e\downarrow)^0(a_1\uparrow)^0(a_1\downarrow)^0]$ (C_{3v}) configuration, and the potential energy curve can be described in terms of S = 1/2, S = 3/2, and S = 5/2 spin states (Figure 7). The $[a_1e^2 \times a_1e^3]$ broken-symmetry curve lies close to the S = 5/2 state at long metal−metal distances, indicating electron localization, whereas at short metal−metal distances, it converges towards the S = 1/2 state where electron delocalization occurs as a result of σ and δ_π bonding. In the intermediate range of metal−metal separations, the S = 3/2 state lies lower in energy than both the S = 1/2 and S = 3/2 states and closest to the broken-symmetry curve. The metal−metal interactions at these intermediate Re−Re distances involve a σ bond but weakly coupled δ_π electrons. The minimum in the broken-symmetry curve for the $[a_1e^2 \times a_1e^3]$ coupling mode is almost coincident with that of the S = 1/2 state (at a Re−Re separation of 2.51−2.52 Å). However, the S = 1/2 and S = 3/2 states are energetically close, with the separation between the respective minima predicted to be only 0.06 eV.

The potential energy curves for the states which are most important for determining the ground state of $[Re_2Cl_9]^{2-}$ are collected in section (b) of Figure 7. The global minimum is predicted to occur at a Re−Re separation of 2.51−2.52 Å, in good agreement with the experimental observation of 2.47 Å,[12] and corresponds to the S = 1/2 state arising from the $[a_1e^2 \times a_1e^3]$ coupling mode, which is characterized by electron delocalization and multiple metal−metal bonding, with a formal bond order of 2.5 (corresponding to $[1.0\ \sigma + 1.5\ \delta_\pi]$).

The potential energy curve for the S = 1/2 state is the lowest-lying curve at metal−metal distances shorter than approximately 2.6 Å but becomes increasingly destabilized at longer Re−Re bond lengths. In the intermediate range of metal−metal distances investigated (corresponding approximately to 2.6−2.9 Å), the S = 3/2 state belonging to the $[a_1e^2 \times a_1e^3]$ coupling mode lies lowest in energy, but the S = 5/2 state arising from the $[a_1e^2 \times a_1^2e^2]$ coupling mode becomes energetically favored at longer Re−Re separations. For clarity, the S = 5/2 curve from the $[a_1e^2 \times a_1e^3]$ coupling mode is not shown, but this state is also favored at Re−Re distances beyond 3.5 Å.

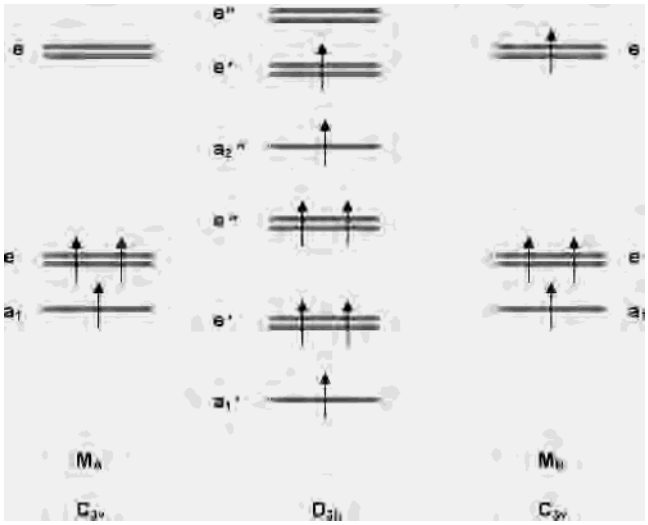

Figure 9. Schematic representation of the electronic configuration for the S = 7/2 state arising from the $[a_1e^2 \times a_1e^3]$ coupling mode of d^3d^4 $[M_2Cl_9]^{2-}$ systems.

As discussed for $[W_2Cl_9]^{2-}$, the $[a_1e^2 \times a_1^2e^2]$ and $[a_1e^2 \times a_1e^3]$ S = 5/2 states of the d^3d^4 dimers are both characterized by a formal metal−metal bond order of 0.5, but the former involves σ bonding and has a shorter metal−metal distance than the latter, which involves δ_π bonding (Table 3).

3.3.2. General Results for $[Tc_2Cl_9]^{2-}$ and $[Mn_2Cl_9]^{2-}$. The behavior of $[Tc_2Cl_9]^{2-}$ shows some similarities to the Re system, but there are also important differences. As found for $[Re_2Cl_9]^{2-}$, the S = 1/2 and S = 3/2 states belonging to the $[a_1e^2 \times a_1e^3]$ coupling mode are energetically close, but in this case the minimum in the S = 3/2 curve has a slightly lower energy. In addition, the S = 5/2 state arising from the $[a_1e^2 \times a_1^2e^2]$ coupling mode is predicted to have the same energy as the $([a_1e^2 \times a_1e^3])$ S = 3/2 state.

The calculations on $[Tc_2Cl_9]^{2-}$ therefore suggest that this system should exhibit two minima (Figure 8), occurring at Tc−Tc separations of 2.66 and 2.99 Å (Table 3), and corresponding, respectively, to the S = 3/2 state from the $[a_1e^2 \times a_1e^3]$ coupling mode and the S = 5/2 state from the $[a_1e^2 \times a_1^2e^2]$ coupling mode. The $([a_1e^2 \times a_1e^3])$ S = 3/2 state contains a single Tc−Tc σ bond and some degree of δ_π bonding, whereas the $([a_1e^2 \times a_1^2e^2])$ S = 5/2 state has electrons in both the bonding (a_1') and antibonding (a_2'') orbitals and therefore a formal Tc−Tc σ bond order of 0.5, and the δ_π electrons are completely localized.

The properties of the Mn system are significantly different from those of the Tc and Re dimers, as an additional state (which is not important for the discussion of $[Tc_2Cl_9]^{2-}$ and $[Re_2Cl_9]^{2-}$) has to be considered (Figure 8). This is the S = 7/2 state arising from the coupling of metal centers with (d^4) high-spin configurations (Figure 9), which can be represented as $[(a_1)^1(e)^2(e)^1]$ (in C_{3v} symmetry).

The S = 7/2 state can be connected with a broken-symmetry configuration equivalent to that for the $[a_1e^2 \times a_1e^3]$ coupling mode. This is a consequence of the fact that

Table 4. Comparison of Calculated and Formal Properties for Odd and Even Electron $[W_2Cl_9]^{z-}$and $[Re_2Cl_9]^{z-}$ Systems

$[W_2Cl_9]^{z-}$	d^3d^3	d^2d^3	d^2d^2
W−W distance	2.43 Å	2.56 Å	2.67 Å
W−W formal bond order	$1.0\sigma + 2.0\,\delta_\pi$	$1.0\sigma + 1.5\,\delta_\pi$	$1.0\,\sigma + 1.0\,\delta_\pi$
W formal oxidation state	+3.0	+3.5	+4.0
W Voronoi charge	+1.34	+1.44	+1.53
$[Re_2Cl_9]^{z-}$	d^3d^3	d^3d^4	d^4d^4
Re−Re distance	2.72 Å	2.52 Å	2.57 Å
Re−Re formal bond order	$1.0\sigma + 2.0\,\delta_\pi$	$1.0\sigma + 1.5\,\delta_\pi$	$1.0\,\sigma + 1.0\,\delta_\pi$
Re formal oxidation state	+4.0	+3.5	+3.0
Re Voronoi charge	+1.41	+1.32	+1.23

both e′ and e″ (D_{3h}) orbitals transform as the e (C_{3v}) irreducible representation when the molecular symmetry is reduced from D_{3h} to C_{3v}. Thus, the broken-symmetry configurations for the low-spin (S = 1/2, S = 3/2, S = 5/2) and S = 7/2 states are both characterized by an overall electron distribution corresponding to an $[(a_1)^2(e)^4(e)^1]$ orbital occupancy. This broken-symmetry configuration can, therefore, encompass the description of both low-spin and high-spin cases.

The calculations on $[Mn_2Cl_9]^{2-}$ (Table 3) suggest that the minima in the S = 5/2 curve from the $[a_1e^2 \times a_1{}^2e^2]$ coupling mode (at a Mn−Mn separation of 2.9 Å) and in the S = 7/2 curve from the $[a_1e^2 \times a_1e^3]$ coupling mode (at a Mn−Mn distance of 3.2 Å) have largely similar energies, and thus this system may also exhibit a double-mimina feature, as predicted for $[Tc_2Cl_9]^{2-}$.

It is important to note that the d^4 Mn center in the ($[a_1e^2 \times a_1e^3]$) S = 7/2 state has a high-spin configuration, and therefore the orbital degeneracy associated with the single occupancy of the e′ level would be more likely to lead to Jahn−Teller distortions since, unlike the $[W_2Br_9]^{2-}$case previously discussed, these orbitals can be described as "modified e_g" orbitals. In order to explore possible Jahn−Teller distortions, additional calculations have been carried for the S = 7/2 state of $[Mn_2Cl_9]^{2-}$ using C_{2v} symmetry, but (as found for $[W_2Br_9]^{2-}$) only minor structural and energetic differences have been observed.

3.4. Comparison of Odd and Even Electron $[M_2Cl_9]^{z-}$ Systems. The differences in the electronic structure and bonding between odd-electron (mixed-valence) and even-electron (same-valence) $[M_2Cl_9]^{z-}$ systems, involving W and Re, have been discussed in the literature on the basis of comparisons of crystallographic data and results from Xα calculations. A summary of our computational results (obtained from density functional calculations) for d^2d^2, d^2d^3, and d^3d^3 $[W_2Cl_9]^{z-}$ and d^3d^3, d^3d^4, and d^4d^4 $[Re_2Cl_9]^{z-}$ is given in Table 4 and Figure 10.

Cotton and co-workers[11] have pointed out that the (0.12 Å) increase in the W−W distance observed for (d^2d^3) $[W_2Cl_9]^{2-}$ with respect to (d^3d^3) $[W_2Cl_9]^{3-}$, although consistent with a decrease in bond order, cannot be rationalized solely in terms of this phenomenon and that the increase in average formal oxidation state of the metal atoms could be a more significant factor. A higher oxidation state should result in a contraction of the metal d orbitals and stronger repulsive forces between the W atoms, thereby weakening the W−W bond.

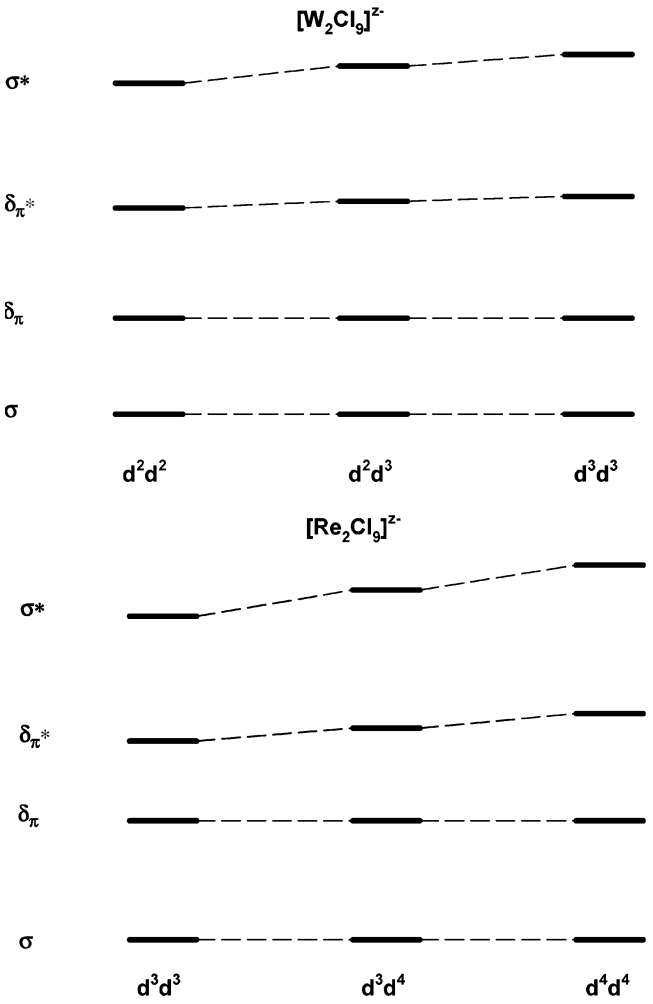

Figure 10. Calculated $\sigma-\sigma^*$ and $\delta_\pi-\delta_\pi^*$ gaps for odd and even electron $[W_2Cl_9]^{z-}$ and $[Re_2Cl_9]^{z-}$ systems. Results correspond to calculations performed at the optimized geometry of the (d^3d^3) S = 0 states.

In addition to the d^2d^3 and d^3d^3 W systems, the crystal structure of the (d^2d^2) $[W_2Cl_9]^{1-}$ dimer has been reported recently[23] and is characterized by a metal−metal distance of 2.70 Å. Our calculations are in good agreement with this result and indicate that the ground state for this system is a delocalized spin-triplet state involving a metal−metal double (σ and δ_π) bond, as previously found for the analogous (d^2d^2) Nb and Ta $[M_2Cl_9]^{3-}$ dimers[3].

Heath and co-workers[12] have compared (d^3d^4) $[Re_2Cl_9]^{2-}$ with (d^3d^3) $[Re_2Cl_9]^{1-}$ and have suggested that the (0.27 Å) decrease in the Re−Re distance, observed for the mixed-valence species, can be explained on the basis that the metal−metal interaction is enhanced due to diminished electrostatic repulsion, stronger σ bonding, and the presence of a significant δ_π bonding contribution in the d^3d^4 system but not in (d^3d^3) $[Re_2Cl_9]^{1-}$.

The observed crystallographic changes for $[W_2Cl_9]^{3-}$, $[W_2Cl_9]^{2-}$, and $[W_2Cl_9]^{1-}$, and the structural differences between $[Re_2Cl_9]^{1-}$ and $[Re_2Cl_9]^{2-}$ are all correctly repro-

(23) Kolesnichenko, V.; Swenson, D. C.; Messerle, L. *Chem. Commun.* **1998**, 2137.

duced by the present calculations (Table 4). The trends displayed by the computational (Voronoi) charges mirror the variation in formal metal oxidation states, but the overall changes across both (W and Re) series are rather small, suggesting that electrostatic effects may be a relatively minor factor.

The analysis of the bonding properties of the $[W_2Cl_9]^{z-}$ and $[Re_2Cl_9]^{z-}$ species indicates that the changes in both σ and δ_π interactions and formal metal−metal bond orders should play an important role in rationalizing the metal−metal bond length differences across the W and Re series. In particular, the present results suggest that the δ_π orbitals should make a greater contribution than originally proposed on the basis of the earlier Xα results.[11]

The $\sigma-\sigma^*$ and $\delta_\pi-\delta_\pi^*$ gaps (obtained from our density functional calculations) for the $[W_2Cl_9]^{z-}$ and $[Re_2Cl_9]^{z-}$ dimers are plotted in Figure 10. Due to the differences in the total molecular charge, it is not possible to use absolute energy values, but if the σ and δ_π levels are chosen as a reference, then the positions of the σ^* and δ_π^* levels provide a measure of the changes in the magnitude of the $\sigma-\sigma^*$ and $\delta_\pi-\delta_\pi^*$ splittings, respectively.

The diagrams in Figure 10 show a significant change in the $\sigma-\sigma^*$ gaps, suggesting a weakening of the metal−metal σ interactions as the formal oxidation states increase from d^3d^3 to d^2d^2 $[W_2Cl_9]^{z-}$ and from d^4d^4 to d^3d^3 $[Re_2Cl_9]^{z-}$. These diagrams also reveal that the magnitude of the $\delta_\pi-\delta_\pi^*$ gaps is significant, and therefore the bonding character of the δ_π orbitals should be sufficiently strong to be an important factor in understanding the trends in metal−metal bond lengths.

In the $[W_2Cl_9]^{z-}$ series, the formal W−W bond order decreases from 3.0 to 2.0 and the $\sigma-\sigma^*$ gap diminishes by approximately 7−9% as the formal oxidation state of the W atoms increases from +3.0 to +4.0. Thus, the changes in the strength of the σ interaction and in metal−metal bond order act conjointly to result in a lengthening of the calculated W−W distance from 2.43 to 2.67 Å.

In the $[Re_2Cl_9]^{z-}$ series, the differences in the magnitude of the $\sigma-\sigma^*$ splittings are larger, with the gap predicted to increase by approximately 15−18% between (d^3d^3) $[Re_2Cl_9]^{1-}$ and (d^4d^4) $[Re_2Cl_9]^{3-}$. However, unlike the W series, the changes in the strength of the σ interaction and in metal−metal bond order work in opposition to one another across the Re series. The expected increase in Re−Re distance for (d^3d^4) $[Re_2Cl_9]^{2-}$ with respect to (d^4d^4) $[Re_2Cl_9]^{3-}$, on the basis of the weakening in Re−Re σ bonding, appears to be counteracted by the increase in formal Re−Re bond order, and the net result is a shortening of the calculated metal−metal bond length from 2.57 to 2.52 Å.

The opposite result emerges from a comparison of the d^4d^4 and d^3d^3 Re dimers. Although a shorter Re−Re distance would be predicted for $[Re_2Cl_9]^{1-}$ relative to $[Re_2Cl_9]^{3-}$, on the basis of an increase in formal bond order from 2.0 to 3.0, the calculated metal−metal bond length actually increases by approximately 0.15 Å. Therefore, in this case, the weakening of the metal−metal σ interaction appears to be more important in determining the metal−metal bond length than changes in the metal−metal bond order.

Previous studies[2] of $[Re_2Cl_9]^{1-}$ have revealed that the global minimum in the broken-symmetry potential energy curve can be described as involving delocalized σ electrons but weakly coupled (or localized) δ_π electrons, corresponding to the antiferromagnetically coupled counterpart of the S = 2 state. Therefore, although the d^3d^3 configuration can accommodate a Re−Re triple bond, the metal−metal interaction in this species is best described as corresponding to a single (σ) bond.

Calculations on the S = 0 state of $[Re_2Cl_9]^{1-}$, which is characterized by complete delocalization of both σ and δ_π electrons leading to multiple metal−metal bonding (and the expected formal bond order of 3.0), indicate that the Re−Re distance in this case is 2.49 Å. This is shorter than the Re−Re bond in (d^3d^4) $[Re_2Cl_9]^{2-}$, but the difference is only 0.03 Å. This result is therefore consistent with the changes in the strength of σ bonding and in metal−metal bond order both having important (but opposite) effects across the $[Re_2Cl_9]^{z-}$ series.

In contrast to (d^3d^3) $[Re_2Cl_9]^{1-}$, the minima in the potential energy curve for the broken-symmetry state of (d^4d^4) $[Re_2Cl_9]^{3-}$ and (d^3d^4) $[Re_2Cl_9]^{2-}$ do correspond to multiply bonded structures, the ground states being delocalized triplet and doublet states, respectively.

In addition to the 5d−5d dimers, where the formation of metal−metal bonds is a predominant factor, it is also interesting to compare the behavior of the analogous 3d−3d systems, namely $[Cr_2Cl_9]^{z-}$ and $[Mn_2Cl_9]^{z-}$. In these species, the metal centers tend to be weakly coupled and have a greater preference for electron localization.

Some interesting observations emerge from a comparison of odd (d^2d^3 and d^3d^4) and even electron (d^3d^3) Cr and Mn dimers. The ground state for the latter is the S = 3 state characterized by complete localization of σ and δ_π electrons. In the case of the mixed-valence species (Tables 2 and 3), calculations predict that the ground state should be the S = 5/2 state where the δ_π electrons are also localized, but a single σ electron can in principle delocalize over the two metal centers leading to some metal−metal bonding (Figures 3 and 6). The calculated Cr−Cr and Mn−Mn distances for the corresponding broken-symmetry states show a decrease of 0.12 and 0.17 Å, respectively, in the (mixed-valence) d^2d^3 and d^3d^4 systems relative to the (same-valence) d^3d^3 systems.

An analysis of the molecular orbital compositions indicates that the single σ electron in the mixed-valence dimers should be 20 to 25% delocalized over the two Cr or Mn centers. Therefore, this (partial) σ-bonding interaction is likely to be associated with the shortening of the metal−metal distance predicted for mixed-valence (d^2d^3) $[Cr_2Cl_9]^{2-}$ and (d^3d^4) $[Mn_2Cl_9]^{2-}$, compared to the respective d^3d^3 ($[Cr_2Cl_9]^{3-}$ and $[Mn_2Cl_9]^{-}$) dimers.

4. Conclusion

The electronic structures and metal−metal bonding in (Cr, Mo, W) d^2d^3 and (Mn, Tc, Re) d^3d^4 $[M_2Cl_9]^{2-}$ systems have been investigated by calculating potential energy curves for various broken-symmetry and other spin states arising from the d^2d^3 and d^3d^4 coupling modes. For the experimentally

known systems ($[Mo_2Cl_9]^{2-}$, $[W_2Cl_9]^{2-}$, and $[Re_2Cl_9]^{2-}$), computational results are in good agreement with observations.

The global minima in $[Mo_2Cl_9]^{2-}$ and $[W_2Cl_9]^{2-}$ correspond to the S = 1/2 state arising from the $[a_1e \times a_1e^2]$ coupling mode. This state is characterized by delocalization of the metal-based electrons in relatively short Mo−Mo and W−W multiple bonds, with a formal bond order of 2.5 (corresponding to $[1.0\ \sigma + 1.5\ \delta_\pi]$). In contrast, the global minimum of the $[Cr_2Cl_9]^{2-}$ system is represented by the S = 5/2 state belonging to the $[e^2 \times a_1e^2]$ coupling mode, which involves electron localization and a weak metal−metal interaction, consistent with a relatively long Cr−Cr separation.

The d^2d^3 and d^3d^4 (dimer) configurations are connected through the electron−hole equivalence of the individual d^2 and d^4 configurations. Thus, the $[Re_2Cl_9]^{2-}$ system shows similarities to $[W_2Cl_9]^{2-}$ and, especially, $[Mo_2Cl_9]^{2-}$ in that a preference for metal−metal bonded structures is also observed. Similarities between Mo and Re systems have been previously found in an study of d^3d^3 $[M_2X_9]^{z-}$ dimers and can be considered to reflect the diagonal relationship existing between these two elements in the periodic table. The global minimum for $[Re_2Cl_9]^{2-}$ is predicted to be the S = 1/2 state belonging to the $[a_1e^2 \times a_1e^3]$ coupling mode (with a formal Re−Re bond order of $[1.0\ \sigma + 1.5\ \delta_\pi]$), but with the S = 3/2 state (which has a formal Re−Re bond order of $[1.0\ \sigma + 0.5\ \delta_\pi]$) lying energetically close (as also observed for $[Mo_2Cl_9]^{2-}$).

In the case of $[Tc_2Cl_9]^{2-}$ and $[Mn_2Cl_9]^{2-}$, two low-lying states have largely similar energy, and thus both systems are predicted to exhibit a double-minima behavior. For the Tc dimer, these correspond to the $([a_1e^2 \times a_1e^3])$ S = 3/2 state (with a formal Tc−Tc bond order of 1.5) and the $([a_1e^2 \times a_1^2e^2])$ S = 5/2 state (with a formal Tc−Tc bond order of 0.5), whereas for the Mn dimer, the two predicted minima correspond to the $([a_1e^2 \times a_1e^3])$ S = 7/2 and $([a_1e^2 \times a_1^2e^2])$ S = 5/2 states.

A comparison of computational results across $[W_2Cl_9]^{z-}$ and $[Re_2Cl_9]^{z-}$ series, involving odd and even electron species, has indicated that changes in both the strength of σ bonding and metal−metal bond order play an important role in rationalizing the trends in metal−metal distances. In the W series, these two factors work conjointly, and the W−W distance is found to decrease as the formal W−W bond order increases and the W−W σ interaction becomes stronger. However, in the Re series, the changes in Re−Re σ bonding and formal Re−Re bond order act in opposition to each other, and the Re−Re distances do not follow a regular trend.

The ground states of both odd (d^2d^3 and d^3d^4) and even (d^3d^3) electron $[Cr_2Cl_9]^{z-}$ and $[Mn_2Cl_9]^{z-}$ dimers are characterized by weak coupling between the metal centers, but calculations predict that the global minima for the mixed-valence species occur at a significantly shorter metal−metal distance. This result can be rationalized on the basis that the (S = 3) ground state of the d^3d^3 dimers involves complete delocalization of all metal-based (σ and δ_π) electrons (and thus no metal−metal bonds), whereas in the (S = 5/2) ground state of the mixed-valence systems, partial delocalization of a single σ electron leads to some degree of metal−metal bonding.

Acknowledgment. Financial support from the Australian Research Council is gratefully acknowledged.

IC049503M